RESEARCH
O&G Forum 2024; 34 – 2s: 709 - 715

APPLICATION OF NEUTROSOPHIC SET TRANSFER LEARNING APPROACH TO CLASSIFY MARBURG-VIRUS

A. Sebasthiyar[1], M. Kavitha[2]
[1] Department of Mathematics, Bharath Institute of Higher Education and Research,India.
[2]Department of Mathematics, Bharath Institute of Higher Education and Research,India.
Author Mail: sebasthiyar1984@gmail.com,
Corresponding Author: kavithakathir3@gmail.com

Abstract

Background: This study aimed to People all throughout the Africa are affected significantly by the Marburg-Virus. Preventing and classify the republic of Africa and local spread of this infectious disease requires early detection. Scientists have generally experimented with a wide range of techniques for both person detection and viral analysis.

Methodology: we used a Qualitative Action Research to collect X-rays that identify Marburg-Virus are one of the techniques employed for diagnosis. whether the individual is afflicted. Additionally, in an effort to provide faster and more reliable findings, the researchers tried to apply deep learning techniques.

Materials: This study employed a balanced database gathered from a Marburg-Virus radiography database, along with the Using the Neutrosophic (NS) domain as its foundation, the ResNet-50 module diagnoses Marburg-Virus patients.

Results: According on experimental data, the suggested method outperformed a precision value obtained from 98.25% reliability rate. earlier research projects carried out using the same database.

Conclusion: The technique is a development of the NS significance method of N. E. M. Khalifa et al. give deep transfer learning NS relevance. True (T), False (F), In the NS domain, chest X-ray pictures were defined using and Indeterminate (I) membership sets.

Keywords: Classify. Marburg-Virus, Neutrosophic set, , filoviruses, pathogenesis, , epidemiology, ecology, clinical symptoms,

Introduction

The Marburg virus is an epidemic disease that has recently spread to the United Republic of Tanzania since March 2023. South Africa saw the first known Marburg virus illness outbreak in Africa and the first since the initial pandemic in West Germany and Yugoslavia in 1967. Africa in February of 1975. The discovery of efficient antiviral therapies is essential for lowering deaths and lessening the effects of Marburg virus outbreaks, which can have a mortality rate ranging from 23% to 90%, depending on the particular outbreak. These are other methods for diagnosing the illness, such as blood tests and images from chest X-rays (CXRs).[1],[2] The imaging investigations that are usually used to diagnose and treat Marburg-Virus patients involve computed tomography (CT) scans and computed radiography (CXR). CT scans and chest radiography, on the however, tests are usually more readily available at medical centers and may be interpreted in a quicker manner than Marburg-Virus laboratory testing. Various lung disorders can be monitored and examined with the help of CXR photographs, as has been demonstrated. such as tuberculosis, infiltration, atelectasis, pneumonia, and hernia. The respiratory system is primarily affected by Marburg-Virus. which can lead to acute respiratory distress syndrome and serious pneumonia in severe cases. Most often, individuals with Marburg-Virus infection are diagnosed by chest X-ray imaging [3]. As a result, many research investigations have been carried out on the use of CXR images in Marburg-Virus diagnosis. Applying deep learning (DL) techniques, or sophisticated neural network learning, is one of the modern methods for diagnosing Marburg-Virus infections. Compared to other conventional approaches, the DL methodology has the benefit of mechanically obtaining characteristics from training data and categorizing them accurately [4]. For many processing pictures applications, a classic neural network known as ResNet, short for Residual Networks, provides the foundation. The primary achievement of ResNet was to enable the training of extraordinarily potent neural networks. over 150 layers. ResNet-50 architecture is a popular convolutional neural network (CNN) DL technique with 50 layers for image recognition [5]. In advance of being converted into the Neutrosophic (NS) domain, all CXR images were in the spital domain. Based on NS, the NS comprises NS fuzzy set, NS image, NS topology, NS crisp set, and NS graph theory. Modern preprocessing of pictures is the application of these components to graphic components, which includes picture transformation through the NS domain, three different kinds of pictures make up the NS domain: Falsity (F) pictures Indeterminacy (I) pictures and True (T) pictures [6]. In this study, every one of the three membership (True, False, and Indeterminate) photos were created. The approach used in the present investigation to deal with its recognition of Marburg-

Virus as a challenge with classification depends on the ResNet-50 architecture with respect to the NS domain. The primary benefit of this research is an analysis of how well NS sets built on the ResNet-50 architecture function when working with large databases of pictures to increase overall accuracy and lower the inaccurate classification rate. This is how the rest of the paper is structured. A summary of the associated work is presented in Section 2, along with a comprehensive framework for Marburg-Virus identification which consists of sections like the overview of the database, NS domain picture with the ResNet-50 model presented in Sect. 3. Section 4 contains the investigation's recommendations and findings., along with a comparison with the current methods. Lastly, the work's result is given in Section 5. Marburg-Virus individuals.

Related Work

Plenty of studies on the recognition and identification of Marburg virus outbreaks have been carried out throughout the last two years. Lawton [7], for instance that suggested a Marburg virus recognition strategy from CT lung scans employing the transfer learning architectures of Contrast Limited Adaptive Histogram Equalization and Standard Histogram Equalization. Narin et al. Five neural network-based models (Inception-ResNetV2, InceptionV3, ResNet-50, ResNet101, and ResNet152) that have been pre-trained are suggested for application in coronavirus pneumonia patient diagnosis using CXR radiographs. (8) Three separate binary classifications with four classes (Marburg virus, normal, bacterial pneumonia, and viral pneumonia) were created using five-fold cross-validation. A real-time governed by rules fuzzy reasoning predictor for Marburg virus identification was proposed by Ilyas et al. [9]. By obtaining real-time sensation data from clients through an Internet of Things platform, the suggested methodology detects both symptomatic and asymptomatic Marburg virus patients. In an effort to categorize Marburg virus affected patients, Sharmila and Florinabel [10] used CXR scans and updated CNN and DCGAN models. Hira & Co. [11] analyzed Marburg virus patients using nine techniques for transfer learning. ResNet-50 outperformed other methods in Marburg virus recognition, producing the optimal outcomes for binary and multi-classes, according to the experiment's conclusions. Saiz and Barandiaran [12] proposed a completely new testing protocol to determine whether a patient has an infection with the Marburg virus by using the SDD300 model. Singh et al. [13] introduced the deep feature in addition SVM-based method for using CXR pictures to detect coronavirus-infected individuals. Instead of using DL-based machine learning algorithms, which need an extensive database for validation and training purposes, SVM was used for categorization. Helwan et al. [14] presented a transferable approach to learning that uses ResNet-18, ResNet-50, and DenseNet-201 to diagnose Marburg virus -positive patients and differentiate between them and people who are healthy. 2715 chest CT scans, both Marburg virus and non- Marburg virus, were used in this study. A better Inception-ResNetV2 DL model was put forth by Alruwaili et al. [15] to diagnose chest CXR pictures with accuracy. Additionally, To improve the visualization of lung infection locations in CXR scans, a Grad-CAM technique was calculated. Using CXR images, Aradhya and colleagues [16] proposed a method for Marburg recognition of viruses. Within the framework of DL architectures, a novel idea of cluster-based oneshot learning was developed. The suggested schema was a multi-class categorization strategy that divided pictures into four groups: influenza virus, influenza bacterial, Marburg virus, and routine cases. The recommended schema is built using an ensemble of Generalized Regression Neural Network and Probabilistic Neural Network classifiers. [17]

3. Material And Methodology

In this work, an effort was put forward to create the Marburg-Virus recognition and detection system depicted in Fig. 1. To extract just Regions, all CXR pictures were first Regions of Interest (ROI) and shrunk during the preliminary stage.

Truth Intermediate Falsity

Figure (1) NS Domain

In the second stage, the three membership subgroups' NS domains were created using the RGB color images as inputs. After that, the method split the NS photos into sets to be used for training and testing using the Resnet-50 model in an 84:16 ratios. After that, the CXR pictures are categorized by the system using Resnet-50. Finally, certain commonly accepted metrics such as F-score, accuracy, sensitivity, specificity, precision, and Matthews Correlation Coefficient (MCC) values, were used to assess the performance of the suggested system [18] [19]. The next subsections provided the specifics of the suggested methodology.

Marburg-Virus Registry

The foundation of any automated method is the database structure. As a result, a database based on the publicly accessible Marburg-Virus radiography database was made. The 21165 CXR images in the database are divided into 10192 normal photos, 3616 Marburg-Virus positive images, 6012 lung opacity images (a lung infection unrelated to Marburg virus), and 1345 cases of viral pneumonia. 7252 CXR pictures (Fig. 2), 3617 of which had a positive Marburg-Virus diagnostic and 3635 of which were randomly selected negatives to produce the balanced database, comprise the data for this paper.

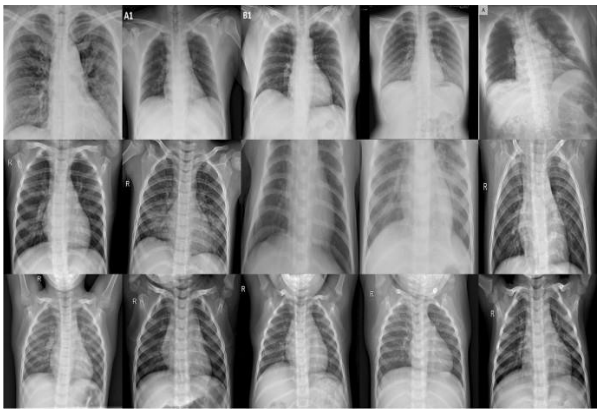

Figure (2) Classification of Marburg-Virus pictures

Information is transformed into a language that is comprehensible to artificial intelligence algorithms. It is

frequently utilized to reduce the complexity of the model and boost its accuracy. Picture information is transformed through a wide range of methods. Thus, the bounding box cropping approach is computed in this step to determine simply the ROI by removing the unwanted environment from the original picture. Initially, the compressed CXR photos are scaled to a set size of 256 × 256 pixels before being imported into the suggested framework.

3.3 Picture in the NS Domain

In 1980, F.Smarandache founded the philosophical field of neutrosophy. It increased the scope of dialectics and investigated the creation, nature, and applications of neutralities as well as their interactions with various ideational spectrums. Advanced image processing approaches include picture conversion into the NS domain, which consists of three areas: experience identification for the background objects, border surveillance for boundary objects, and backdrop reduction for protagonist objects. Every event has a distinct degree of falsity (F), indeterminacy (I), and truth (T). every single one of which require to be considered independently, pursuant to the concept of neutrosophy. The NS truth domain shows each image's true portion as a percentage. The picture is then referred to as an actual picture. Additionally, the NS falsehood degree of membership exposes the inaccurate portions of the picture and turns them into an image that's separate from the rest of the picture.[20],[21] The parts of all unclear pictures that include the lowest amount of data from the original picture are called the NS indeterminacy membership degree [22], [23]. The picture is represented as a mathematical object (Spatial Domain) by a M * N matrix. By using mathematical equations (1)–(3) for determining It is feasible to convert each pixel P (p, q) from the picture domain into an NS domain, such that PNS (p, q) = T (p, q), I (p, q), and F (p, q). The likelihood [24] that pixel P (p, q) belongs to the white set (item), indeterminate set, and non-white set (the backdrop), respectively, is here denoted by T (p, q), I (p, q), and F (p, q) (Fig. 1).

$$T(p,q) = \frac{\overline{\sigma}(p,q) - \overline{\sigma}_{min}}{\overline{\sigma}_{max} - \overline{\sigma}_{min}} \quad (1)$$

$$I(p,q) = \frac{\eta(p,q) - \eta_{min}}{\eta_{max} - \eta_{min}} \quad (2)$$

$$F(p,q) = 1 - T(p,q) = \frac{\overline{\sigma}_{max} - \overline{\sigma}(p,q)}{\overline{\sigma}_{max} - \overline{\sigma}_{min}} \quad (3)$$

where: • σ (p, q) represents a picture's intensity of the pixels value.

• In the NS domain, T, I, and F are true, indeterminacy, and false sets, correspondingly.

• The neighborhood mean value of σ (p, q) is represented by $\overline{\sigma}$ (p, q).

• The consistency rating of T at (p, q) is represented by the symbol η(p, q), which is the absolute ratio between the local mean value $\bar{\sigma}$(p, q) as well as the concentration value σ (p, q) of a picture.

3.4 The model of the Deep Residual Neural Network (ResNet-50)

Artificial neural networks are used in deep learning (DL), a machine learning technique for learning representations. Supervised, semi-supervised, and unsupervised machine learning approaches are the three categories of methods [25], [26]. A computer model is able to learn to do tasks such as categorization directly from text, visual, or numeric data by using deep learning (DL). For classification tasks, extraction of deep features is typically used with neural networks that have been trained like DenseNet-201, Xception Net, MobileNetV2, ShuffleNet, ResNet18, ResNet-50, ResNet-101, InceptionV3, InceptionResNet-V2, AlexNet, VGG16, VGG19, GoogleNet, and ResNet-18 [4]. ResNet-50, an improved version of CNN, was used in this study as the foundational model in the suggested scheme of architecture to categorize CXR pictures of Marburg-Virus and normal patients.

The database maintained by ImageNet served as the model's pre-training source for item detection. ResNet reduces interference, which arises as the size of the network increases in depth and complexity, by using shortcuts between layers [27]. The network terminates with a 1051 fully linked layer upon The Soft Max algorithm activation. With 24,543,473 trainable parameters, there are a total of 52 weighted layers [28], [29]. ResNet-50, a set of more than 14 million photos categorized into more than 20,052 groups for visual recognition contests, was trained using the ImageNet database [8].

4. Experimental Findings and Discussion:

The suggested framework's primary goal is to categorize CXR pictures as either normal or Marburg virus. In this part, we randomly split the repository into an 84% training set and a 16% testing set. This allowed ResNet-50 to be trained on a dataset of 7235 pictures as a reference set and implemented for every subgroup, namely, CXR pictures in the NS Domain. On a Windows 10 PC with an Intel Core i7 processor and 16 GB of RAM, the suggested approach was put into practice for Marburg-Virus diagnosis using the MATLAB R2020a computational language.

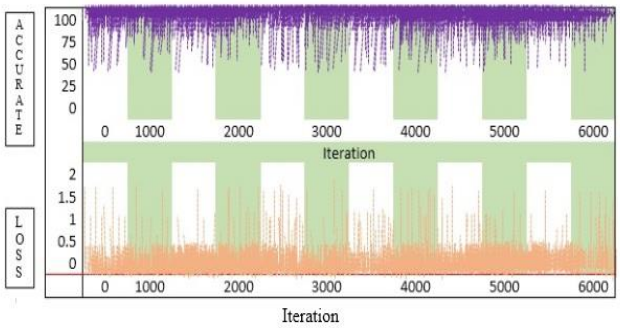

Figure (3) The accuracy and loss curves of the suggested model that resulted from the T-Domain.

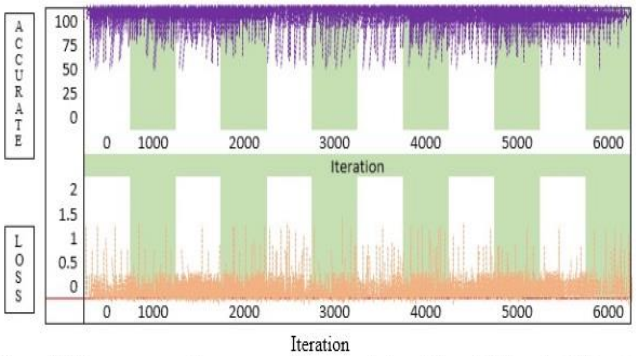

Figure (4) The accuracy and loss curves of the suggested model resulted from the F-Domain.

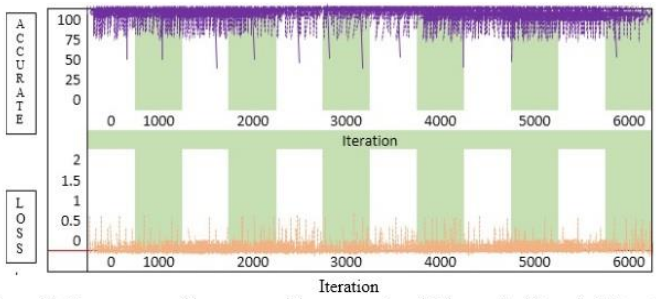

Figure (5) The accuracy and loss curves of the suggested model that resulted from the I-Domain.

Weight updates, five epochs, and a 1e-4 learning rate were all performed with the Adam optimizer; the same Mini Batch Size was utilized at each stage. Using this technique, pictures are converted to NS domains, each of which has a different epoch. as illustrated by the precision of the accuracy and loss curves in Figs. 3-5 for each of the three domains.

Furthermore, a thorough set of experiments was conducted to assess the suggested framework's accomplishments in terms of the matrix of confusion measurements, specifically the MCC rates, F-score, accuracy, sensitivity, specificity, and precision. A table illustrating an algorithm's categorization for information is called a confusion matrix. As seen in Fig. 7, Four sections formed the framework of the confusion matrix: Positive True, Positive False, Negative True, and Negative False. As a result, the database's pictures were assessed in the NS domain using various confidence levels for a chosen model, the ResNet-50 model, which had been developed using five epochs: epochs 5, 10, 15, 20, and 25. Ultimately, we compute the mean for every domain and overlay it with the mean of various other domains.

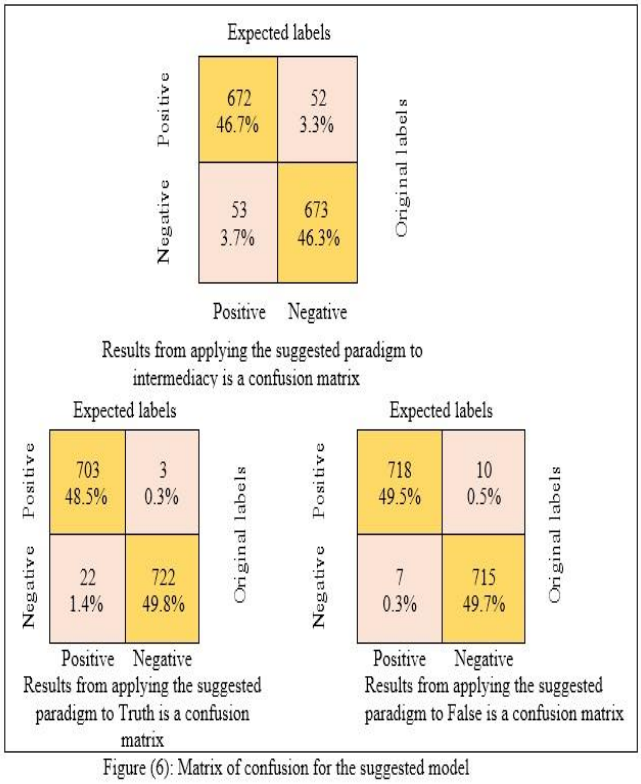

Figure (6): Matrix of confusion for the suggested model

Table 1 illustrates Accuracy of total epoch evaluation on the empirical data set, which was approximately 97.73% in the F-domain. Moreover, Table 2 shows that Sensitivity Assessment of all epochs combined in the T-domain was 98.04 %. As shown in Tables 3 shows that Specificity of evaluation throughout all eras 98.30% in the F-domain.

TABLE 1: Accuracy of total epoch evaluation

Number of generations						
NS Membership	**VP24**	**VP30**	**VP35**	**VP40**	**L**	**Average (%)**
T	96.86	96.54	97.43	96.86	96.54	96.84
F	97.15	96.88	98.13	98.54	97.98	**97.73**
I	86.17	88.99	90.94	89.81	92.23	89.62

Epochs 5, 10, 15, 20 and 25 are referred to as EP5, EP10, EP15, EP20 and EP25, respectively. The top outcome for each row is bolded.

TABLE 2: Sensitivity Assessment of all epochs combined

Number of generations						
NS Membership	**EP5**	**EP10**	**EP15**	**EP20**	**EP25**	**Average (%)**
T	96.34	97.96	99.71	98.25	97.94	**98.04**
F	97.13	95.65	97.32	97.25	95.47	96.56
I	84.61	87.67	89.61	87.90	90.22	88.00

Epochs 5, 10, 15, 20 and 25 are referred to as EP5, EP10, EP15, EP20 and EP25, respectively. The top outcome for each row is bolded.

TABLE 3: Specificity of evaluation throughout all eras

Number of generations						
NS Membership	**EP5**	**EP10**	**EP15**	**EP20**	**EP25**	**Average (%)**
T	97.60	97.74	96.17	96.43	96.34	96.85
F	97.72	98.68	96.82	98.95	99.33	**98.30**
I	93.72	88.74	91.41	92.32	93.44	91.92

Epochs 5, 10, 15, 20 and 25 are referred to as EP5, EP10, EP15, EP20 and EP25, respectively. The top outcome for each row is bolded.

TABLE 4: Assessment of the whole epochs' precision

Number of generations						
NS Membership	**EP5**	**EP10**	**EP15**	**EP20**	**EP25**	**Average (%)**

T	98.52	97.76	97.25	96.45	96.73	97.34
F	97.92	99.14	97.57	99.76	99.54	**98.78**
I	93.28	89.72	92.64	91.78	92.81	92.04

Epochs 5, 10, 15, 20 and 25 are referred to as EP5, EP10, EP15, EP20 and EP25, respectively. The top outcome for each row is bolded.

TABLE 5: Assessment of the whole epochs' F-Score

Number of generations						
NS Membership	**EP5**	**EP10**	**EP15**	**EP20**	**EP25**	**Average (%)**
T	96.71	97.54	97.12	96.98	97.92	97.25
F	98.82	98.92	98.20	98.75	96.93	**98.32**
I	86.84	89.38	89.61	90.31	92.54	89.73

Epochs 5, 10, 15, 20 and 25 are referred to as EP5, EP10, EP15, EP20 and EP25, respectively. The top outcome for each row is bolded.

TABLE 6: Assessment of MCC across all eras

Number of generations						
NS Membership	**EP5**	**EP10**	**EP15**	**EP20**	**EP25**	**Average (%)**
T	94.70	94.39	95.51	95.47	94.74	94.96
F	96.03	95.31	95.53	96.15	97.64	**96.13**
I	76.21	77.71	80.83	79.73	85.69	80.03

Epochs 5, 10, 15, 20 and 25 are referred to as EP5, EP10, EP15, EP20 and EP25, respectively. The top outcome for each row is bolded.

TABLE 7: Assessing the status of the art today with pertinent studies

Articles	Methods	Database	Percentage of accuracy
Afifi *et al*. [28]	CNN-DenseNet161	11,196 CXR Pictures	91.20
Abd Elaziz *et al*. [29]	MobileNetV3+Aqu	21155 CXR Pictures	92.40
Ahmad and Wady [30]	CT, GWT, and LGIP	7252 CXR Pictures	96.18
Walvekar and Shinde [31]	ResNet-50	359 CXR Pictures	96.23
Apostolopoulos and Mpesiana [32]	MobileNetv2	1427 CXR Pictures	96.78
Proposed	ResNet-50+NS	7253 CXR Pictures	**98.25**

Tables 4 shows that Specificity of evaluation throughout all eras are 98.78%. in the F-domain. Tables 5 shows that Assessment of the whole epochs' accuracy are 98.32%. in the F-domain. Tables 6 shows that Assessment of MCC across all eras are 96.13%. in the F-domain. Lastly, Table 7 compares the outcomes of the suggested approach to a few cutting-edge methods. achieved the best outcome using ResNet-50. This is because the model was able to demonstrate better accuracy to the combination of the NS Domain and ResNet-50 techniques. In addition, compared to earlier research, the best result was attained with an overall accuracy of 98.25%..in the Proposed method.

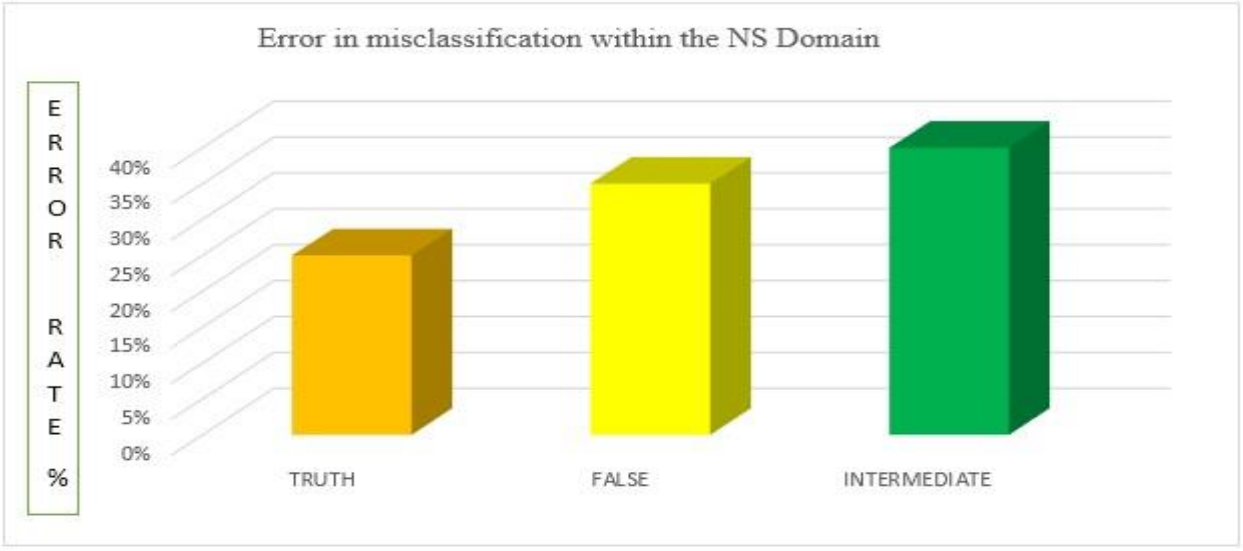

Figure (7) Error in misclassification within the NS Domain

The incorrect categorization rate of errors metric was also used to examine the performance of the suggested scenarios using a comparable information and processing environment. The erroneous classification error rates for the suggested situations were computed, as shown in Fig. 7. The outcomes confirmed that the suggested scenario performs significantly better than all other scenarios, with a slight misclassification error of 1.95% rate in the ResNet-50 Falsity domain. As a result, this situation was taken into consideration as a possible Marburg Virus. CXR Picturee categorization technique.

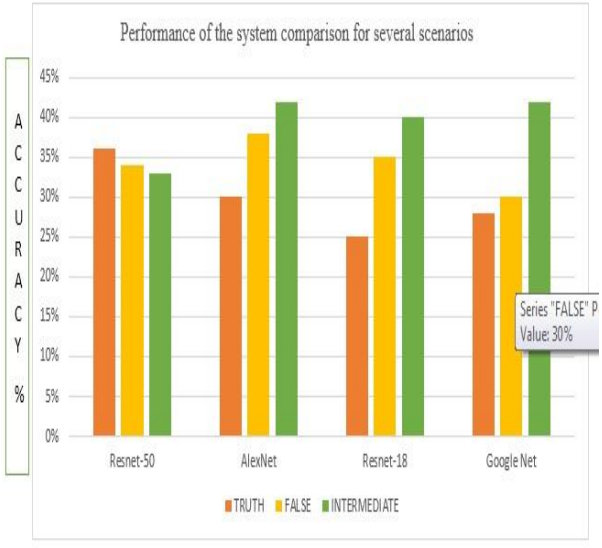

Figure (8) Performance of the system comparison for several scenarios

The suggested solution outperformed other techniques in terms of results, especially average precision when classification. The results of the publication [1] and the results of the framework that was proposed have been compared as a last tool for the performance evaluation of the proposed framework, as illustrated in Fig. 8.

5.CONCLUSION

The virus that has destroyed every state in the Africa and put everybody under extreme quarantine is called Marburg-Virus. The Africa stability was threatened by the virus, which also brought about a new era of turmoil and uncertainty. There is still work to be done in terms of using technology to stop and the virus from spreading by Classifying how they are affected. The goal of the study done on this paper is to benefit the public and make it easier for Marburg-Virus specialists to classify patients. The NS set's basic ideas were used in the investigation. True (T), Indeterminacy (I), and Falsity (F) photographs from the CXR picture dataset that corresponded to each Marburg-Virus and ordinary persons are included in the regulations. This study differs from the others in that the gathered pictures were converted into an NS domain trained on the DL approach, and it was trained on the data set using ResNet-50 as a transfer learning method. Consequently, the model's average accuracy score of 98.25% exceeded the accuracy scores of other experiments conducted on a comparable database.

References

1. *Marburg Virus Disease. Available online: https://www.who.int/news-room/fact-sheets/detail/marburg-virus-disease (accessed on 4 May 2023).*
2. *Kuhn, J.H.; Amarasinghe, G.K.; Basler, C.F.; Bavari, S.; Bukreyev, A.; Chandran, K.; Crozier, I.; Dolnik, O.; Dye, J.M.; Formenty, P.B.H.; et al. ICTV Virus Taxonomy Profile: Filoviridae. J. Gen. Virol.* ***2019****, 100, 911–912. [Google Scholar] [CrossRef]*
3. *Towner, J.S.; Pourrut, X.; Albariño, C.G.; Nkogue, C.N.; Bird, B.H.; Grard, G.; Ksiazek, T.G.; Gonzalez, J.-P.; Nichol, S.T.; Leroy, E.M. Marburg Virus Infection Detected in a Common African Bat. PLoS ONE* ***2007****, 2, e764. [Google Scholar] [CrossRef] [PubMed]*
4. *Almeida, F.C.; Giannini, N.P.; Simmons, N.B. The Evolutionary History of the African Fruit Bats (Chiroptera:*

Pteropodidae). Acta Chiropterologica ***2016****, 18, 73–108. [Google Scholar] [CrossRef]*

1. *Gordon Smith, C.E.; Simpson, D.I.H.; Bowen, E.T.W.; Zlotnik, I. Fatal Human Disease from Vervet Monkeys. Lancet* ***1967****, 290, 1119–1121. [Google Scholar] [CrossRef] [PubMed]*
2. *Kissling, R.E.; Robinson, R.Q.; Murphy, F.A.; Whitfield, S.G. Agent of Disease Contracted from Green Monkeys. Science* ***1968****, 160, 888–890. [Google Scholar] [CrossRef]*
3. *Marburg Virus Disease—Equatorial Guinea. Available online: https://www.who.int/emergencies/disease-outbreak-news/item/2023-DON449 (accessed on 3 May 2023).*
4. *Marburg Virus Disease—United Republic of Tanzania. Available online: https://www.who.int/emergencies/disease-outbreak-news/item/2023-DON451 (accessed on 3 May 2023).*
5. *Marzi, A.; Feldmann, H. Marburg Virus Disease: Global Threat or Isolated Events? J. Infect. Dis.* ***2023****, 228, 103–105. [Google Scholar] [CrossRef]*
6. *Hickman, M.R.; Saunders, D.L.; Bigger, C.A.; Kane, C.D.; Iversen, P.L. The Development of Broad-Spectrum Antiviral Medical Countermeasures to Treat Viral Hemorrhagic Fevers Caused by Natural or Weaponized Virus Infections. PLoS Negl. Trop. Dis.* ***2022****, 16, e0010220. [Google Scholar] [CrossRef]*
7. *Bradfute, S.B. The Discovery and Development of Novel Treatment Strategies for Filoviruses. Expert Opin. Drug Discov.* ***2022****, 17, 139–149. [Google Scholar] [CrossRef]*
8. *Bukreyev, A.A.; Volchkov, V.E.; Blinov, V.M.; Dryga, S.A.; Netesov, S.V. The Complete Nucleotide Sequence of the Popp (1967) Strain of Marburg Virus: A Comparison with the Musoke (1980) Strain. Arch. Virol.* ***1995****, 140, 1589–1600. [Google Scholar] [CrossRef] [PubMed]*
9. *Leung, D.W.; Prins, K.C.; Basler, C.F.; Amarasinghe, G.K. Ebolavirus VP35 Is a Multifunctional Virulence Factor. Virulence* ***2010****, 1, 526–531. [Google Scholar] [CrossRef] [PubMed][Green Version]*
10. *Liu, G.; Nash, P.J.; Johnson, B.; Pietzsch, C.; Ilagan, M.X.G.; Bukreyev, A.; Basler, C.F.; Bowlin, T.L.; Moir, D.T.; Leung, D.W.; et al. A Sensitive in Vitro High-Throughput Screen To Identify Pan-Filoviral Replication Inhibitors Targeting the VP35–NP Interface. ACS Infect. Dis.* ***2017****, 3, 190–198. [Google Scholar] [CrossRef][Green Version]*
11. *Hasan, M.; Mia, M.M.; Islam, M.M.; Hasan Saraf, M.S.; Islam, M.S. A Computerized Pharmaceutical Repurposing Approach Reveals Semicochliodinol B Synthesized from Chrysosporium Merdarium as a Viable Therapeutic Contender for Marburg Virus's VP35 and VP40 Proteins. Inform. Med. Unlocked* ***2022****, 28, 100821. [Google Scholar] [CrossRef]*
12. *16. Bale, S.; Julien, J.-P.; Bornholdt, Z.A.; Kimberlin, C.R.; Halfmann, P.; Zandonatti, M.A.; Kunert, J.; Kroon, G.J.A.; Kawaoka, Y.; MacRae, I.J.; et al. Marburg Virus VP35 Can Both Fully Coat the Backbone and Cap the Ends of DsRNA for Interferon Antagonism. PLoS Pathog.* ***2012****, 8, e1002916. [Google Scholar] [CrossRef] [PubMed]*
13. *17. Heikamp, K.; Bajorath, J. The Future of Virtual Compound Screening. Chem. Biol. Drug Des.* ***2013****, 81, 33–40. [Google Scholar] [CrossRef] [PubMed]*
14. *18. Lill, M. Virtual Screening in Drug Design. In In Silico Models for Drug Discovery; Kortagere, S., Ed.; Methods in Molecular Biology; Humana Press: Totowa, NJ, USA, 2013; pp. 1–12. ISBN 978-1-62703-342-8. [Google Scholar]*
15. *19. Fischer, A.; Smieško, M.; Sellner, M.; Lill, M.A. Decision Making in Structure-Based Drug Discovery: Visual Inspection of Docking Results. J. Med. Chem.* ***2021****, 64, 2489–2500. [Google Scholar] [CrossRef]*
16. *20. Eberhardt, J.; Santos-Martins, D.; Tillack, A.F.; .Forli, S. AutoDock Vina 1.2.0: New Docking Methods, Expanded Force Field, and Python Bindings. J. Chem. Inf. Model.* ***2021****, 61, 3891–3898. [Google Scholar] [CrossRef] [PubMed]*
17. *El-Demerdash, A.; Al-Karmalawy, A.A.; Abdel-Aziz, 21.T.M.; Elhady, S.S.; Darwish, K.M.; Hassan, A.H.E. Investigating the Structure–Activity Relationship of Marine Natural Polyketides as Promising SARS-CoV-2 Main Protease Inhibitors. RSC Adv.* ***2021****, 11, 31339–31363. [Google Scholar] [CrossRef]*
18. *22. Tian, W.; Chen, C.; Lei, X.; Zhao, J.; Liang, J. CASTp 3.0: Computed Atlas of Surface Topography of Proteins. Nucleic Acids Res.* ***2018****, 46, W363–W367. [Google Scholar] [CrossRef] [PubMed][Green Version]*
19. *23. M Kavitha, P Murugadas, V Kamalakanan, Picture Fuzzy Matrix for Medical Application Indian Journal Of Natural Sciences 2023. 14 (79), 59472-59478.*
20. *24. Nath, A.; Kumer, A.; Khan, M.W. Synthesis, Computational and Molecular Docking Study of Some 2, 3-Dihydrobenzofuran and Its Derivatives. J. Mol. Struct.* ***2021****, 1224, 129225. [Google Scholar] [CrossRef]*
21. *25. Cosconati, S.; Forli, S.; Perryman, A.L.; Harris, R.; Goodsell, D.S.; Olson, A.J. Virtual Screening with AutoDock: Theory and Practice. Expert Opin. Drug Discov.* ***2010****, 5, 597–607. [Google Scholar] [CrossRef][Green Version]*
22. *Nath, A.; Kumer, A.; Zaben, F.; Khan, M.W. Investigating the Binding Affinity, Molecular Dynamics, and ADMET Properties of 2,3-Dihydrobenzofuran Derivatives as an Inhibitor of Fungi, Bacteria, and Virus Protein. Beni-Suef Univ. J. Basic Appl. Sci.* ***2021****, 10, 36. [Google Scholar] [CrossRef]*
23. *Rahman, M.M.; Islam, M.R.; Akash, S.; Mim, S.A.; Rahaman, M.S.; Emran, T.B.; Akkol, E.K.; Sharma, R.; Alhumaydhi, F.A.; Sweilam, S.H.; et al. In Silico Investigation and Potential Therapeutic Approaches of Natural Products for COVID-19: Computer-Aided Drug Design Perspective. Front. Cell. Infect. Microbiol.* ***2022****, 12, 929430. [Google Scholar] [CrossRef]*
24. *Biovia, D.S. Discovery Studio Modeling Environment; Dassault Systemes: San Diego, CA, USA, 2015. [Google Scholar]*
25. *29. Cichero, E.; Calautti, A.; Francesconi, V.; Tonelli, M.; Schenone, S.; Fossa, P. Probing In Silico the Benzimidazole Privileged Scaffold for the Development of Drug-like Anti-RSV Agents. Pharmaceuticals* ***2021****, 14, 1307. [Google Scholar] [CrossRef] [PubMed].*